Synthesis of New Visible Light Active Photocatalysts of $Ba(In_{1/3}Pb_{1/3}M'_{1/3})O_3$ (M′ = Nb, Ta): A Band Gap Engineering Strategy Based on Electronegativity of a Metal Component

Su Gil Hur, Tae Woo Kim, and Seong-Ju Hwang*

Center for Intelligent Nano-Bio Materials (CINBM), Division of Nano Sciences and Department of Chemistry, Ewha Womans University, Seoul 120-750, Korea

Hyunwoong Park and Wonyong Choi

School of Environmental Science and Engineering, Pohang University of Science and Technology, Pohang, Kyungbuk 790-784, Korea

Sun Jin Kim and Jin-Ho Choy

Center for Intelligent Nano-Bio Materials (CINBM), Division of Nano Sciences and Department of Chemistry, Ewha Womans University, Seoul 120-750, Korea

Received: April 6, 2005; In Final Form: June 12, 2005

We have synthesized new, efficient, visible light active photocatalysts through the incorporation of highly electronegative non-transition metal Pb or Sn ions into the perovskite lattice of $Ba(In_{1/3}M_{1/3}M'_{1/3})O_3$ (M = Sn, Pb; M′ = Nb, Ta). X-ray diffraction, X-ray absorption spectroscopic, and energy dispersive spectroscopic microprobe analyses reveal that tetravalent Pb or Sn ions exist in the B-site of the perovskite lattice, along with In and Nb/Ta ions. According to diffuse UV−vis spectroscopic analysis, the Pb-containing quaternary metal oxides $Ba(In_{1/3}Pb_{1/3}M'_{1/3})O_3$ possess a much narrower band gap ($E_g \sim 1.48-1.50$ eV) when compared to the ternary oxides $Ba(In_{1/2}M'_{1/2})O_3$ ($E_g \sim 2.97-3.30$ eV) and the Sn-containing $Ba(In_{1/3}Sn_{1/3}M'_{1/3})O_3$ derivatives ($E_g \sim 2.85-3.00$ eV). Such a variation of band gap energy upon the substitution is attributable to the broadening of the conduction band caused by the dissimilar electronegativities of the B-site cations. In contrast to the ternary or the Sn-substituted quaternary compounds showing photocatalytic activity under UV−vis irradiation, the $Ba(In_{1/3}Pb_{1/3}M'_{1/3})O_3$ compounds induce an efficient photodegradation of 4-chlorophenol under visible light irradiation ($\lambda > 420$ nm). The present results highlight that the substitution of electronegative non-transition metal cations can provide a very powerful way of developing efficient visible light harvesting photocatalysts through tuning of the band structure of a semiconductive metal oxide.

Introduction

Semiconductive metal oxides or metal chalcogenides have received intense research interest for decades because of their activity for the photocatalytic decomposition of organic pollutants and water splitting.[1,2] Such a photodissociation assisted by the photocatalysts starts from an electronic transition from the valence band (VB) to the conduction band (CB) with the generation of electron−hole pairs. Among various semiconducting materials, titanium oxide has been the most intensively investigated material because it has many merits from economic and ecological points of view.[3−5] However, due to its wide band gap ($E_g \sim 3.2$ eV), TiO_2 can absorb only a small fraction of solar energy (about 4% of total energy) and the overall photocatalytic efficiency is usually very low. In this regard, band gap engineering is very important in designing a better photocatalyst. Over the past few decades, there have been several attempts to modify band gap energy. For instance, organic sensitizers are anchored onto the TiO_2 surface to endow visible light activity.[3] Even though such an approach proved to be effective in enhancing photoefficiency, the sensitizer dyes lack for the long-term stability and are not very useful for practical applications. On the other hand, cation or anion substitution into a metal oxide lattice reportedly controlled the band gap energy of the metal oxide semiconductor.[6−8] In particular, a perovskite-structured metal oxide is a good base material for the chemical substitution, since this structure can accommodate diverse component ions into the lattice to form stable solid solutions. Recently, several attempts have been made to synthesize visible light active photocatalysts through the incorporation of transition metal ions into the perovskite lattice of niobate or tantalate.[9] Such studies would be inspired by the visible light absorption property of transition metal ions as well as by the charge-balance consideration of metal substituents. Currently, it is well-established that most of the semiconducting metal oxides possess a VB with 2p states of oxygen and a CB with nd/(n + 1)s states of metal cation.[10] Taking into account the fact that the energy of the electronic level of an element is inversely proportional to its electronegativity,[11] we have made a conjecture that incorporation of an electronegative non-transition metal cation would give rise to the narrowing of the band gap through the lowering of the CB position.

In this work, we have tried to synthesize a new, efficient, visible light active photocatalyst by incorporating highly electronegative Pb^{IV} or Sn^{IV} cations into the perovskite-structured tantalates and niobates. The crystal and band structures of the obtained $Ba(In_{1/3}M_{1/3}M'_{1/3})O_3$ (M = Sn, Pb; M′ = Nb, Ta) compounds have been studied by X-ray diffraction (XRD) and

* To whom correspondence should be addressed. Tel: +82-2-3277-4370. Fax: +82−2−3277−3419. E-mail: hwangsju@ewha.ac.kr.

10.1021/jp051752o CCC: $30.25
Published on Web 07/19/2005

diffuse reflectance UV−vis spectroscopy. The oxidation states and local geometries of the substituted cations were examined with X-ray absorption near-edge structure (XANES) spectroscopy. Their crystallite morphology and chemical composition were probed with field emission scanning electron microscopy (FE-SEM) and energy dispersive spectroscopic microprobe analyses (EDS). The decomposition of organic pollutants under visible or UV−vis irradiation was examined to investigate the photocatalytic activity of the synthesized material.

Experimental Section

Polycrystalline $Ba(In_{1/3}M_{1/3}M'_{1/3})O_3$ and $Ba(In_{1/2}M'_{1/2})O_3$ samples with M = Sn, Pb and M′ = Nb, Ta were prepared by the conventional solid-state reaction with the stoichiometric mixture of $BaCO_3$, In_2O_3, SnO_2, PbO_2, Nb_2O_5, and Ta_2O_5. Except for $Ba(In_{1/3}Pb_{1/3}M'_{1/3})O_3$ composition, high-purity samples could be obtained by calcining the mixture at 800 °C, subsequently sintering at 1000−1130 °C for 4 days with intermittent grindings, and finally slow-cooling to room temperature. In the case of $Ba(In_{1/3}Pb_{1/3}M'_{1/3})O_3$, the above process leads to the formation of a mixture of cubic perovskite and layered perovskite phases. Instead, the cubic perovskite structures could be realized by adopting a thermal shock treatment, in which the mixture of precursors was rapidly introduced into a high-temperature zone of 1100 °C, reacted at this temperature for 6 h, and then abruptly quenched to room temperature. All of the heat treatments performed in this work were done in oxygen atmosphere to stabilize the higher oxidation states of Pb^{IV} and Sn^{IV} and to avoid the formation of lower valent Pb^{II} and Sn^{II} ions as well.

The variation of lattice parameters upon the chemical substitution was examined by XRD measurements using Ni-filtered Cu Kα radiation with a graphite diffracted beam monochromator. The morphology and particle size for all the samples were determined by FE-SEM using a JEOL JSM-6700F microscope. During FE-SEM experiments, semiquantitative EDS analysis was also carried out on several crystallites to confirm the incorporation of Sn or Pb ions into the perovskite lattice. To determine the surface area and porosity, the nitrogen adsorption−desorption isotherms were measured volumetrically at liquid nitrogen temperature. Prior to the adsorption measurement, the calcined samples were degassed at 200 °C for 2 h in a vacuum.

Diffuse reflectance UV−vis spectra were obtained on a Perkin-Elmer Lambda 35 spectrometer equipped with an integrating sphere using $BaSO_4$ as a reference. The recorded reflectance data were used to estimate the band gap energy by converting the reflectance data to absorption data through the Kubelka−Munk function.[12] X-ray absorption spectroscopic (XAS) experiments were carried out at Pb L_{III}-, Sn L_{III}-, Nb K-, and TaL_{III}-edges with the extended X-ray absorption fine structure (EXAFS) facility installed at the beam line 7C at the Pohang Light Sources (PLS) in Korea. XAS data were collected at room temperature in transmission mode using gas-ionization detectors. All the present spectra were calibrated carefully by measuring the spectra of Pb, Sn, Nb, or Ta metal. Data analysis for the experimental spectra was performed with the standard procedure reported previously.[13]

The photocatalytic reactions were carried out in a Pyrex reactor (30 mL) with a quartz window, which was subjected to UV−vis or visible radiation. A 300-W Xe arc lamp (Oriel) was used as a light source. Light passed through a 10-cm IR water filter and a UV cutoff filter ($\lambda > 300$ nm for UV illumination and $\lambda > 420$ nm for visible illumination), then the filtered light was focused onto the reactor. Methylene blue (MB) and 4-chlorophenol (4-CP) were used as test substrates, and their photocatalytic degradation in aqueous catalyst suspensions was monitored as a function of the irradiation time. The evolution of MB concentration was monitored spectrophotometrically by measuring the absorbance at $\lambda = 665$ nm with an UV−vis spectrophotometer (Agilent 8453). The degradation of 4-CP was followed chromatographically by using a reverse-phase high-performance liquid chromatograph (Agilent 1100 series). The eluent consisted of a binary mixture of water containing 0.1% phosphoric acid and acetonitrile (80:20 by volume). The production of chlorides from the degradation of 4-CP was also determined by using an ion chromatograph (IC, Dionex DX-120) that was equipped with a Dionex IonPac AS 14 (4 mm × 250 mm) column and a conductivity detector. The eluent solution was 3.5 mM of Na_2CO_3/1 mM of $NaHCO_3$.

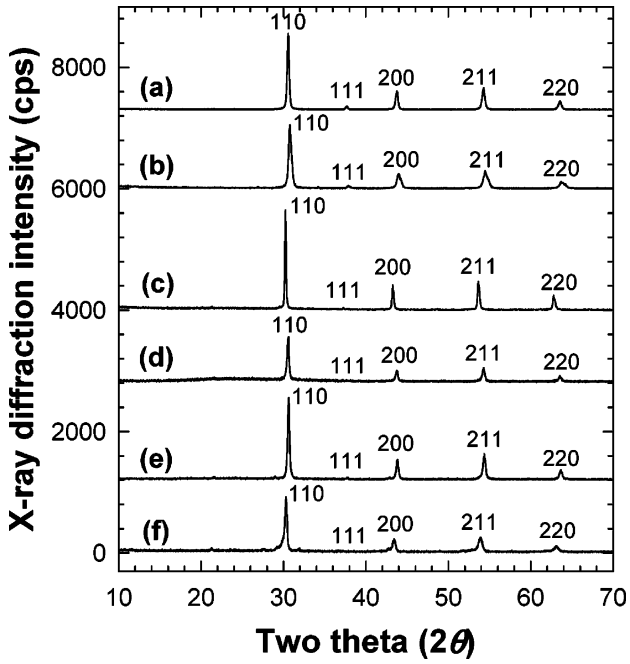

Figure 1. Powder XRD patterns of (a) $Ba(In_{1/2}Nb_{1/2})O_3$, (b) $Ba(In_{1/3}Sn_{1/3}Nb_{1/3})O_3$, (c) $Ba(In_{1/3}Pb_{1/3}Nb_{1/3})O_3$, (d) $Ba(In_{1/2}Ta_{1/2})O_3$, (e) $Ba(In_{1/3}Sn_{1/3}Ta_{1/3})O_3$, and (f) $Ba(In_{1/3}Pb_{1/3}Ta_{1/3})O_3$.

Results and Discussion

Powder XRD Analysis. Figure 1 represents the powder XRD patterns of the quaternary metal oxides $Ba(In_{1/3}M_{1/3}M'_{1/3})O_3$ with M = Sn and Pb and M′ = Nb and Ta, together with those of the ternary $Ba(In_{1/2}M'_{1/2})O_3$ compounds. All of the intense diffraction peaks could be well-indexed on the basis of the perovskite structure with the cubic symmetry.[9] For some compositions, several minor peaks are detectable but their very low intensities (less than 1%) certify that the secondary phase has negligible influence on the overall optical and catalytic properties. According to least-squares fitting analyses, the lattice parameter a increases in the order of $Ba(In_{1/3}Sn_{1/3}M'_{1/3})O_3 < Ba(In_{1/2}M'_{1/2})O_3 < Ba(In_{1/3}Pb_{1/3}M'_{1/3})O_3$, which is in good agreement with the relative size of B-site cations ($Sn^{IV}(6) = 0.83$ Å, $Pb^{IV}(6) = 0.915$ Å, $Nb^{V}(6) = 0.78$ Å, $Ta^{V}(6) = 0.78$ Å, and $In^{III}(6) = 0.94$ Å, where the number in parentheses represents the coordination number).[14] The absence of superlattice lines clarifies the random distribution of Sn/Pb, In, and Nb/Ta ions in the B-site of perovskite lattice. The tolerance factor, $t = (r_A + r_O)/\{2^{1/2}(r_B + r_O)\}$, was calculated for each composition on the basis of the radii of the component ions.[15]

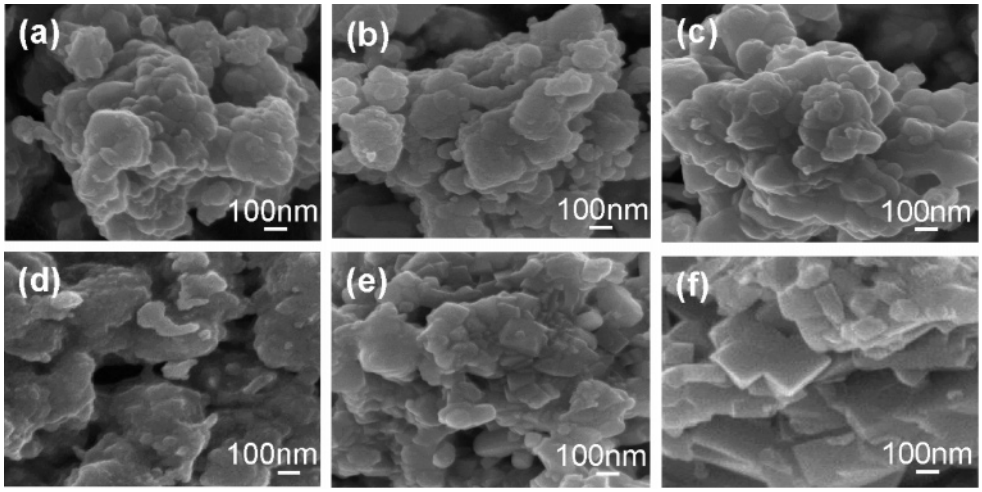

Figure 2. FE-SEM images of (a) $Ba(In_{1/2}Nb_{1/2})O_3$, (b) $Ba(In_{1/3}Sn_{1/3}Nb_{1/3})O_3$, (c) $Ba(In_{1/3}Pb_{1/3}Nb_{1/3})O_3$, (d) $Ba(In_{1/2}Ta_{1/2})O_3$, (e) $Ba(In_{1/3}Sn_{1/3}Ta_{1/3})O_3$, and (f) $Ba(In_{1/3}Pb_{1/3}Ta_{1/3})O_3$.

TABLE 1: Lattice Parameters, Unit Cell Volumes, Tolerance Factors, and Band Gap Energies of $Ba(In_{1/2}M'_{1/2})O_3$ and $Ba(In_{1/3}M_{1/3}M'_{1/3})O_3$ with M = Sn, Pb and M′ = Nb, Ta

sample	*a* (Å)	unit cell volume (Å^3)	tolerance factor, *t*	band gap energy (eV)
$Ba(In_{1/2}Nb_{1/2})O_3$	4.1452	71.226	1.00	3.30
$Ba(In_{1/3}Sn_{1/3}Nb_{1/3})O_3$	4.1377	70.840	1.01	3.00
$Ba(In_{1/3}Pb_{1/3}Nb_{1/3})O_3$	4.1856	73.329	1.00	1.48
$Ba(In_{1/2}Ta_{1/2})O_3$	4.1389	70.901	1.00	2.97
$Ba(In_{1/3}Sn_{1/3}Ta_{1/3})O_3$	4.1367	70.788	1.01	2.85
$Ba(In_{1/3}Pb_{1/3}Ta_{1/3})O_3$	4.1636	72.178	0.99	1.50

As listed in Table 1, these values are within the range of 0.99−1.01, which is in good agreement with the observed cubic symmetry of the present compounds.

FE-SEM, N_2 Adsorption−Desorption Isotherm, and EDS Analyses. The particle size and crystallite morphology of the $Ba(In_{1/3}M_{1/3}M'_{1/3})O_3$ and $Ba(In_{1/2}M'_{1/2})O_3$ compounds were examined by using FE-SEM. As shown in Figure 2, all of the present compounds show a similar morphology with particle sizes of 100−300 nm. There is no systematic change of morphology and crystal size depending on the chemical composition. The EDS analysis was also made to check the chemical composition of the products, confirming the formation of quaternary compounds with the Sn or Pb substituent. The N_2 adsorption−desorption isotherm measurements (not shown) clarify the absence of pores in the present samples, as supposed from their perovskite structure. A surface area calculation based on the BET equation demonstrated that all of the samples under investigation possess only a small surface area of ∼2−4 m^2/g with negligible variations depending on the chemical composition.

XANES Analysis. The oxidation states of the substituted Pb and Sn ions have been carefully examined by performing XANES spectroscopy at the Pb L_{III}- and Sn L_{III}-edges, since these elements have two different stable oxidation states of +2 and +4. The Pb L_{III}-edge XANES spectra for the $Ba(In_{1/3}Pb_{1/3}Nb_{1/3})O_3$ and $Ba(In_{1/3}Pb_{1/3}Ta_{1/3})O_3$ compounds are presented in Figure 3, in comparison with those of the references PbO and PbO_2. The selection rule for photoelectric excitation in the dipolar approximation predicts that the transitions to final states with orbital angular momentum quantum number l_f, which is different from the initial state with l_i by ±1 unit, are allowed.[16] Since the tetravalent lead ions possess vacant 6s and 6d orbitals, the reference $Pb^{IV}O_2$ shows not only the main-edge peaks A and B corresponding to $2p_{3/2} \rightarrow 6d$ transitions but also the pre-edge peak P corresponding to the $2p_{3/2} \rightarrow 6s$ transition.[17] On the contrary, such an intense pre-edge peak P is absent in the reference spectrum of divalent PbO with a Pb electronic configuration of [Xe] $4f^{14}5d^{10}6s^2$. As shown in Figure 3, both perovskite-structured materials exhibit a distinct pre-edge peak P, evidence of the tetravalent oxidation state of Pb in these compounds. This is cross-confirmed by the similar edge positions of $Ba(In_{1/3}Pb_{1/3}M'_{1/3})O_3$ and the reference $Pb^{IV}O_2$, which are higher than that of the reference $Pb^{II}O$. Taking into account the fact that the lead ion in the perovskite compounds is stabilized in an octahedral environment, we were able to assign the lower energy to peak A and the higher one to B as a $2p_{3/2} \rightarrow 6d_{t_{2g}}$ and a $2p_{3/2} \rightarrow 6d_{e_g}$ transition, respectively.[17] The energy difference between peaks A and B appears almost identical for both perovskite compounds, indicating a similar chemical environment of lead ions in these samples.

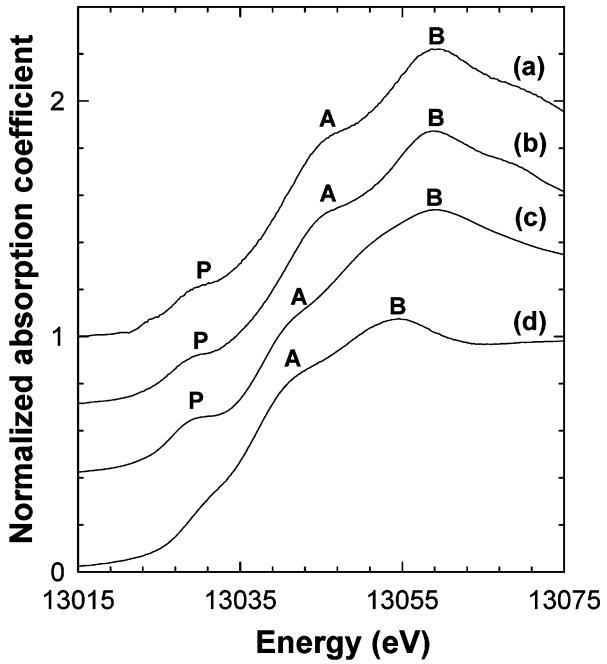

Figure 3. Pb L_{III}-edge XANES spectra for (a) $Ba(In_{1/3}Pb_{1/3}Nb_{1/3})O_3$ and (b) $Ba(In_{1/3}Pb_{1/3}Ta_{1/3})O_3$, in comparison with the reference spectra for (c) PbO_2 and (d) PbO.

Figure 4 represents the Sn L_{III}-edge XANES spectra of $Ba(In_{1/3}Sn_{1/3}M'_{1/3})O_3$ and the references SnO and SnO_2. Even

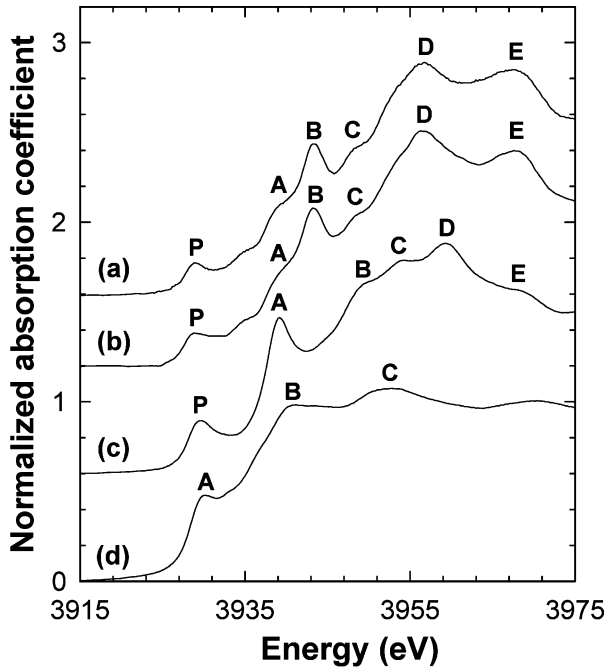

Figure 4. Sn L_{III}-edge XANES spectra for (a) $Ba(In_{1/3}Sn_{1/3}Nb_{1/3})O_3$ and (b) $Ba(In_{1/3}Sn_{1/3}Ta_{1/3})O_3$, in comparison with the reference spectra for (c) SnO_2 and (d) SnO.

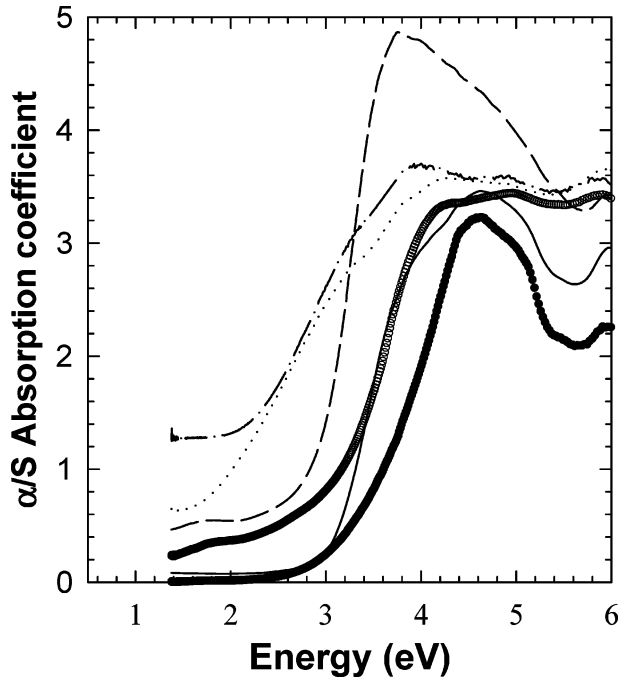

Figure 5. Diffuse reflectance UV−vis spectra for $Ba(In_{1/2}Nb_{1/2})O_3$ (open circles), $Ba(In_{1/3}Sn_{1/3}Nb_{1/3})O_3$ (solid lines), $Ba(In_{1/3}Pb_{1/3}Nb_{1/3})O_3$ (dotted lines), $Ba(In_{1/2}Ta_{1/2})O_3$ (closed circles), $Ba(In_{1/3}Sn_{1/3}Ta_{1/3})O_3$ (dashed lines), and $Ba(In_{1/3}Pb_{1/3}Ta_{1/3})O_3$ (dot−dashed lines).

though the spectral features in the main-edge region (denoted as A, B, C, D, and E) seem to be strongly dependent on the local crystal structure around tin atoms in each compound, the energies of the edge jump and main-edge peaks of $Ba(In_{1/3}Sn_{1/3}M'_{1/3})O_3$ are similar to those of the reference $Sn^{IV}O_2$ but higher than those of the reference $Sn^{II}O$, indicating the tetravalent oxidation state of tin in the perovskite-structured materials. Moreover, the pre-edge peak P corresponding to the $2p_{3/2} \rightarrow 5s$ transition appears with a similar spectral weight for both $Ba(In_{1/3}Sn_{1/3}M'_{1/3})O_3$ and SnO_2, which reflects the unoccupied 5s state of tetravalent tin atoms in these materials. On the contrary, such a transition is not allowed for the reference $Sn^{II}O$ due to the full occupancy of the final Sn 5s orbital. In this regard, despite the similar energy between peak A of the reference $Sn^{II}O$ and peak P of the other tetravalent compounds, peak A in the former should be assigned as a transition to unoccupied 5d states, as supported from its much greater intensity. As can be seen from Figure 4, both the $Ba(In_{1/3}Sn_{1/3}Nb_{1/3})O_3$ and $Ba(In_{1/3}Sn_{1/3}Ta_{1/3})O_3$ exhibit nearly the same spectral shape and peak positions, implying a similar chemical environment of tin ions in these samples. Summarizing the present XANES results, we were able to conclude that the heat treatment in $P_{O_2} = 1$ atm was really effective in stabilizing high-valent Pb^{IV} or Sn^{IV} ions in the perovskite lattice of tantalates and niobates. Since the electronegativity of an element is strongly dependent on its oxidation state,[18] it is very important to stabilize the tetravalent oxidation states of the lead or tin ion in realizing the present band gap engineering strategy based on the electronegativity of metal cations. In addition, we have probed the chemical environments of Nb and Ta ions by using Nb K- and Ta L_{III}-edge XANES analyses (see Supporting Information). In the Nb K-edge region, all of the niobium-containing samples show a weak pre-edge peak P corresponding to a $1s \rightarrow 4d$ transition. Since this transition is forbidden by the dipole selection rule for the absorber ions in octahedral sites,[16] the observed weak intensity of this pre-edge peak clarifies the stabilization of niobium ions in the octahedral B-site of the perovskite lattice. In the case of Ta L_{III}-edge XANES data, a clear splitting of main-edge peaks A and B appears in the energy range of 9884−9889 eV for all the Ta-based oxides under investigation. From their relative intensities and their positions, we were able to assign them as the transitions of $2p_{3/2} \rightarrow 5d_{t_{2g}}$ and $2p_{3/2} \rightarrow 5d_{e_g}$, respectively. Such spectral features provide clear evidence on the existence of Ta ions in regular octahedral sites. Furthermore, there are no marked spectral differences at both edges between $Ba(In_{1/3}M_{1/3}M'_{1/3})O_3$ and $Ba(In_{1/2}M'_{1/2})O_3$, implying the negligible influences of Sn and Pb substitution on the chemical environment of Nb and Ta.

Diffuse UV−vis Spectroscopy. The UV−vis spectra of the $Ba(In_{1/3}M_{1/3}M'_{1/3})O_3$ compounds are illustrated in Figure 5, together with those of $Ba(In_{1/2}M'_{1/2})O_3$. The band gap energies of these compounds were evaluated by the linear interpolation of α/S absorption coefficients.[12] The ternary metal oxides $Ba(In_{1/2}M'_{1/2})O_3$ were found to be wide band gap semiconductors with $E_g = 2.97-3.30$ eV. As summarized in Table 1, the incorporation of Pb ions significantly reduced the E_g value from around 3 to 1.48−1.50 eV, which is much smaller than the E_g value of niobium- or tantalum-based oxide (>4.0 eV).[10] In contrast, the incorporation of Sn ions only slightly reduced E_g. This finding provides clear evidence of the narrowing of the band gap energy through chemical substitution, which endows the resulting materials with visible light harvesting ability. Such a modification of band structure upon the cation substitution can be explained on the basis of the high electronegativity of the metal substituent. That is, the band structure of a metal oxide semiconductor consists of metal nd/(n + 1)s and O 2p levels which form CB and VB, respectively.[10] In the case of the pristine strontium indium niobate, the band gap energy is related to the energy difference between In 5s and O 2p states. Considering that the substituted Pb^{IV} and Sn^{IV} ions are more electronegative than the In^{III} ion,[18,19] the Pb 6s and Sn 5s states are expected to have lower energy than that of the In 5s state, which leads to a lowering of CB and the narrowing of band gap separation; see Figure 6. The fact that the lead substitution effect on E_g was far greater than the tin substitution effect is consistent with the

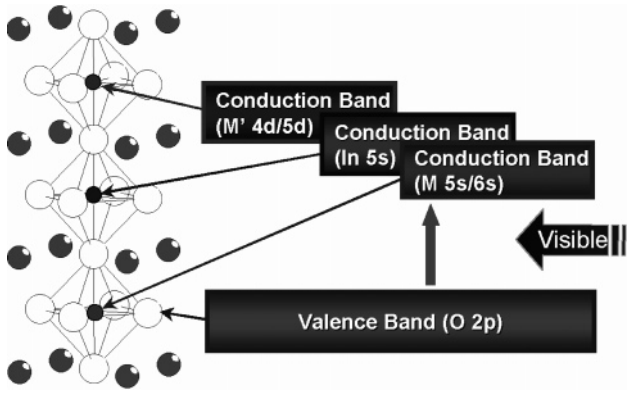

Figure 6. Schematic model for the variation of band structure of $Ba(In_{1/3}M_{1/3}M'_{1/3})O_3$ (M = Sn, Pb; M′ = Nb, Ta) induced by the incorporation of tetravalent lead or tin cations.

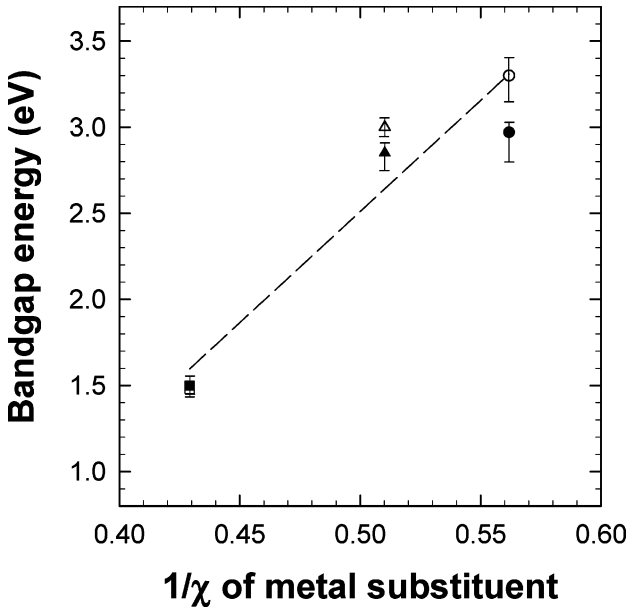

Figure 7. Plot of band gap energy vs the inverse electronegativity of substitutent Pn/Sn/In cations for $Ba(In_{1/2}Nb_{1/2})O_3$ (open circles), $Ba(In_{1/3}Sn_{1/3}Nb_{1/3})O_3$ (open triangles), $Ba(In_{1/3}Pb_{1/3}Nb_{1/3})O_3$ (open squares), $Ba(In_{1/2}Ta_{1/2})O_3$ (closed circles), $Ba(In_{1/3}Sn_{1/3}Ta_{1/3})O_3$ (closed triangles), and $Ba(In_{1/3}Pb_{1/3}Ta_{1/3})O_3$ (closed squares). The dashed line represents a linear regression line for all the present data.

fact that Pb^{IV} is more electronegative than Sn^{IV}.[19] As shown in Figure 7, we have plotted the band gap energy of the present samples as a function of the inverse electronegativity of the substituted In^{III}, Sn^{IV}, or Pb^{IV} ions. Both factors display roughly a linear relationship ($E_g = 12.91\chi_{Pauling}^{-1} - 3.95$), although the types of metal orbital contributing to CB are different from the In/Sn 5s orbital to the Pb 6s one. This finding verifies that the inverse electronegativity of the substituent cation can be a semiquantitative measure for tailoring the band gap energy of transition metal oxide.

Photocatalytic Activity Measurement. We have evaluated the photocatalytic activities of the present perovskite-type oxides by measuring the photodegradation of MB and 4-CP under UV−vis or visible light irradiation (see Figures 8 and 9). Figure 8 shows that the lead-substituted $Ba(In_{1/3}Pb_{1/3}M'_{1/3})O_3$ compounds possess significant visible light activity for the degradation of 4-CP whereas the pristine $Ba(In_{1/2}M'_{1/2})O_3$ and their tin-substituted derivatives are completely inactive under visible light irradiation ($\lambda > 420$ nm). A near stoichiometric production of chloride occurs concurrently with the degradation of 4-CP (see Figure 8b), which confirms that the removal of 4-CP is indeed

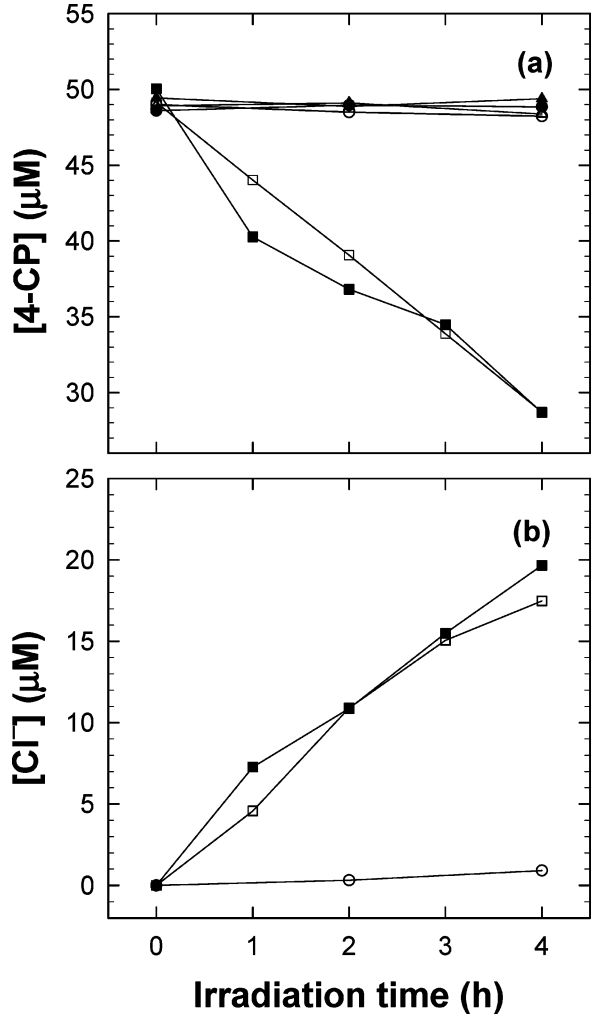

Figure 8. Variation of concentration of (a) 4-chlorophenol and (b) evolved chloride species upon photoreaction with visible light radiation ($\lambda > 420$ nm) for $Ba(In_{1/2}Nb_{1/2})O_3$ (open circles), $Ba(In_{1/3}Sn_{1/3}Nb_{1/3})O_3$ (open triangles), $Ba(In_{1/3}Pb_{1/3}Nb_{1/3})O_3$ (open squares), $Ba(In_{1/2}Ta_{1/2})O_3$ (closed circles), $Ba(In_{1/3}Sn_{1/3}Ta_{1/3})O_3$ (closed triangles), and $Ba(In_{1/3}Pb_{1/3}Ta_{1/3})O_3$ (closed squares).

due to the visible light induced degradation, not to the adsorption. The detection of CO and CO_2 gases that evolved during the photodegradation of 4-CP can provide further evidence of the visible light driven photolysis of the organic molecules by the lead-substituted compounds (see Supporting Information). Such visible light photocatalytic activity is surely ascribed to the band gap narrowing upon the incorporation of the electronegative cation. On the other hand, the fact that the incorporation of Sn into the perovskite lattice fails to induce any visible light activity is consistent with the result that the tin substitution influenced the band gap less than the lead one (Table 1). Such different activities depending on the kind of cation substituents can be well understood on the basis of the dissimilar electronegativities of Pb^{IV} and Sn^{IV} ions.[19] In fact, the $Ba(In_{1/3}Sn_{1/3}Ta_{1/3})O_3$ possesses a rather smaller E_g value (2.85 eV) than the threshold wavelength limit of 420 nm corresponding to $E = 2.95$ eV applied for the examination of visible active photocatalysis. But this compound does not induce visible light driven photocatalysis of 4-CP, as shown in Figure 8. We have suggested that this would originate from a slightly higher VB position of $Ba(In_{1/3}Sn_{1/3}Ta_{1/3})O_3$ than the oxidation potential of 4-CP, since the narrowing of the band gap upon Sn substitution is not sufficient. In this case, the absorption of visible light radiation does not guarantee the visible light driven

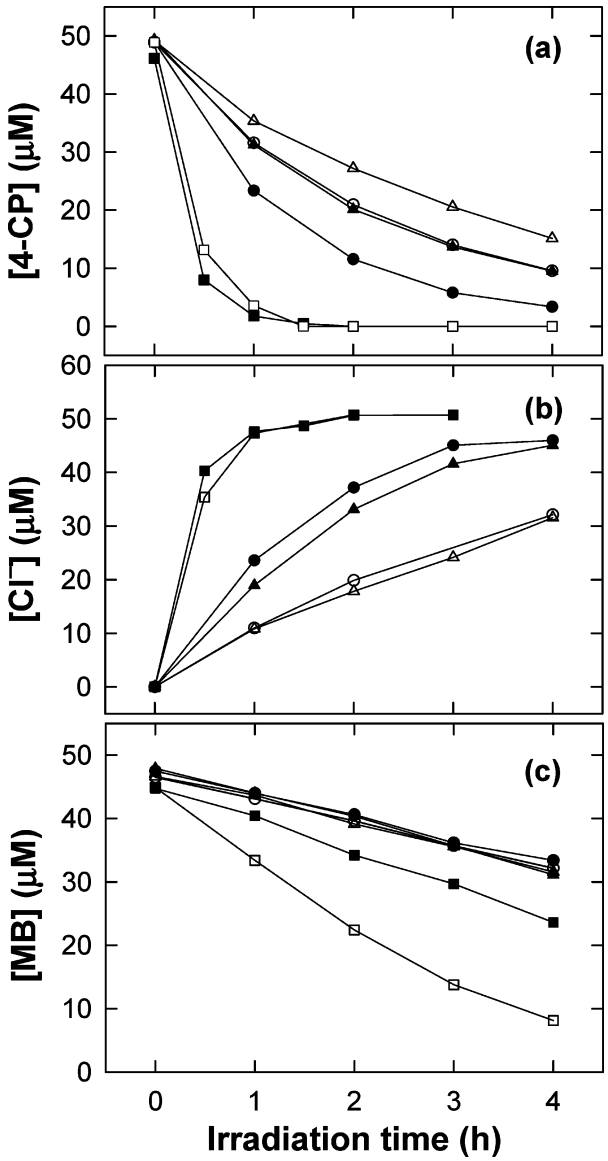

Figure 9. Variation of concentration of (a) 4-chlorophenol, (b) evolved chloride species, and (c) methylene blue upon photoreaction with UV−vis radiation (λ > 300 nm) for $Ba(In_{1/2}Nb_{1/2})O_3$ (open circles), $Ba(In_{1/3}Sn_{1/3}Nb_{1/3})O_3$ (open triangles), $Ba(In_{1/3}Pb_{1/3}Nb_{1/3})O_3$ (open squares), $Ba(In_{1/2}Ta_{1/2})O_3$ (closed circles), $Ba(In_{1/3}Sn_{1/3}Ta_{1/3})O_3$ (closed triangles), and $Ba(In_{1/3}Pb_{1/3}Ta_{1/3})O_3$ (closed squares).

photolysis of the organic species. In this regard, it is necessary to sufficiently reduce the E_g value of transition metal oxide for creating visible light active photocatalytic activity with respect to diverse volatile organic compounds. We also carried out the photolysis experiments under an UV−vis irradiation (λ > 300 nm) condition and present the results in Figure 9. The rate of 4-CP degradation was much faster under the UV−vis irradiation, and the lead-substituted derivatives exhibit the highest activity as in the case of visible irradiation. The discoloration of MB under UV−vis irradiation, which is widely used as a test reaction of photocatalytic activity, is also compared and shows a similar trend (Figure 9c). Once again, the tin substitution does not improve the photoactivity of the pristine $Ba(In_{1/2}M'_{1/2})O_3$ even in the presence of UV light. The above results demonstrate that the lead substitution generates the visible light activity without sacrificing the UV activity. It is often observed that metal cation substitution induces the visible light activity but few changes or even decreases in the UV activity occur because the energy levels of the metal dopants located within the band gap could serve as a recombination center. This is undesirable from a practical point of view and successful solar applications of visible light active material that should utilize both visible and UV light efficiently. In summary, the substitution of In/Ta/Nb ions with a more electronegative Pb^{IV} ion was found to be very effective in providing wide band gap semiconducting materials with the visible light activity by lowering the CB position.

Conclusion

Efficient, visible light driven photocatalysts of the perovskite-structured $Ba(In_{1/3}Pb_{1/3}M'_{1/3})O_3$ (M′ = Nb, Ta) were successfully prepared by the incorporation of electronegative non-transition metal cations into UV-active, wide band gap, semiconductive materials. According to the XRD, XANES, EDS, and diffuse reflectance UV−vis reflectance spectroscopic analyses, tetravalent Pb or Sn ions are successfully incorporated into the B-site of the perovskite lattice, resulting in significant narrowing of the band gap. As expected from the higher electronegativity of Pb^{IV} ion than those of Sn^{IV} and In^{III} ions, the Pb-substituted derivatives show a greater photocatalytic activity under visible and UV−vis irradiations, compared to ternary $Ba(In_{1/2}M'_{1/2})O_3$ and quaternary $Ba(In_{1/3}Sn_{1/3}M'_{1/3})O_3$ compounds (M′ = Nb, Ta). The present findings underline that the band gap energy and photocatalytic activity of semiconducting material can be effectively controlled by the substitution of non-transition metal ions with high electronegativity. This work provides strong evidence that electronegativity can be a qualitative measure for selecting an appropriate substituent cation to create efficient visible light active photocatalysts. Recently we have found that an incorporation of more electronegative Bi^V ions is even more powerful for the band gap narrowing of a semiconducting metal oxide than Pb^{IV} substitution. Such findings provide strong support for the importance of electronegativity in the design of visible light harvesting materials for the application of photocatalysts and electrodes for the solar cell.

Acknowledgment. This work was supported by Grant No. R08-2003-000-10409-0 from the Basic Research Program of the Korea Science & Engineering Foundation. The experiments at Pohang Light Source (PLS) were supported in part by MOST and POSTECH.

Supporting Information Available: Nb K- and Ta L_{III}-edge XANES spectra of $Ba(In_{1/2}M'_{1/2})O_3$ and $Ba(In_{1/3}M_{1/3}M'_{1/3})O_3$ (M = Sn, Pb; M′ = Nb, Ta) and some references. Time-dependent plot of the concentrations of CO and CO_2 gases evolved during the photodegradation of 4-CP by the lead-substituted compound. This material is available free of charge via the Internet at http://pubs.acs.org.

References and Notes

(1) Honda, K.; Fujishima, A. *Nature* **1972**, *238*, 37.

(2) (a) Hoffmann, M. R.; Martin, S. T.; Choi, W.; Bahnemann, D. W. *Chem. Rev.* **1995**, *95*, 69. (b) Mills, A.; Hunte, S. L. *J. Photochem. Photobiol. A* **1997**, *108*, 1.

(3) (a) Vlachopoulos, N.; Liska, P.; Augustynski, J.; Gratzel, M. *J. Am. Chem. Soc.* **1988**, *110*, 1216. (b) Bae, E.; Choi, W.; Park, J.; Shin, H. S.; Kim, S. B.; Lee, J. S. *J. Phys. Chem. B* **2004**, *108*, 14093.

(4) Schlafani, A.; Mozzanega, M. N.; Pichat, P. *J. Photochem. Photobiol. A* **1991**, *59*, 181.

(5) (a) Sato, T.; Yamamoto, Y.; Fujishiro, Y.; Uchida, S. *J. Chem. Soc., Faraday Trans.* **1996**, *92*, 5089. (b) Choy, J. H.; Lee, H. C.; Jung, H.; Hwang, S. J. *J. Mater. Chem.* **2001**, *11*, 2232.

(6) (a) Zou, Z.; Ye, J.; Sayama, K.; Arakawa, H. *Nature* **2001**, *414*, 625. (b) Anpo, M. *Bull. Chem. Soc. Jpn.* **2004**, *77*, 1427. (c) Choi, W.; Termin, A.; Hoffmann, M. R. *J. Phys. Chem.* **1994**, *98*, 13669.

(7) (a) Anpo, M. *Pure Appl. Chem.* **2000**, *72*, 1265−1270. (b) Anpo, M.; Takeuchi, M. *J. Catal.* **2003**, *216*, 505−516. (c) Anpo, M., Corma, A.,

et al., Eds. 12th International congress on Catalysis. *Studies in Surface Science and Catalysis*; Elsevier: Amsterdam, 2000; Vol. 130, p 157, and the references therein.

(8) Asahi, R.; Morikawa, T.; Ohwaki, T.; Aoki, K.; Taga, Y. *Science* **2001**, *293*, 269.

(9) (a) Yin, J.; Zou, Z.; Ye, J. *J. Phys. Chem. B* **2003**, *107*, 4936. (b) Hwang, D. W.; Kim, H. G.; Lee, J. S.; Kim, J.; Li, W.; Oh, S. H. *J. Phys. Chem. B* **2005**, *109*, 2093.

(10) (a) Yin, J.; Zou, Z.; Ye, J. *J. Phys. Chem. B* **2003**, *107*, 61. (b) Tang, J.; Zou, Z.; Ye, J. *Chem. Mater.* **2004**, *16*, 1644.

(11) Huheey, J. H.; Keiter, E. A.; Keiter, R. L. *Inorganic Chemistry: Principles of Structure and Reactivity*; HarperCollins: New York, 1993; p 171.

(12) Marking, G. A.; Hanko, J. A.; Kanatzidis, M. G. *Chem. Mater.* **1998**, *10*, 1191.

(13) Choy, J. H.; Hwang, S. J.; Park, N. G. *J. Am. Chem. Soc.* **1997**, *119*, 1624.

(14) Shannon, R. D. *Acta Crystallogr. A* **1976**, *32*, 751.

(15) Yoo, J.; Lee, Y.; Yoon, K.; Hwang, S.; Suh, S.; Kim, J.; Yoo, C. *Jpn. J. Appl. Phys.* **2001**, *40*, 3256.

(16) Teo, B. K. *EXAFS: Basic Principles and Data Analysis*; Springer-Verlag: Berlin, Germany, 1986.

(17) Rao, K. J.; Wong, J. *J. Chem. Phys.* **1984**, *81*, 4832−4843.

(18) (a) Pauling, L. *The Nature of the Chemical Bond*, 3rd ed.; Cornell University: Ithaca, NY, 1960; p 93. (b) Allred, A. L. *J. Inorg. Nucl. Chem.* **1961**, *17*, 215.

(19) Electronegativity of the component metal cations from ref 18: $\chi_{Pauling}(In^{III}) = 1.78$, $\chi_{Pauling}(Nb^{V}) = 1.6$, $\chi_{Pauling}(Sn^{IV}) = 1.96$, and $\chi_{Pauling}(Pb^{IV}) = 2.33$.